ELSEVIER

Chemical Engineering Journal 138 (2008) 283–294

Chemical Engineering Journal

www.elsevier.com/locate/cej

Experimental and numerical study on stagnation point offset of turbulent opposed jets

Li Weifeng *, Sun Zhigang, Liu Haifeng, Wang Fuchen, Yu Zunhong

Key Laboratory of Coal Gasification, Ministry of Education, East China University of Science and Technology, P.O. Box 272, Shanghai 200237, People's Republic of China

Received 11 January 2007; received in revised form 14 May 2007; accepted 17 May 2007

Abstract

The stagnation point offsets of turbulent opposed jets at various exit velocity ratios and nozzle separations were experimentally studied by a hot-wire anemometer, smoke-wire technique and numerically simulated by Reynolds stress model (RSM). Results show that for $2D \leq L \leq 4D$ (where L is nozzle separation and D is nozzle diameter), the position of the impingement plane is unstable and oscillates within a region between two relative stable positions when the exit velocities are equal. However, the impingement plane deviates from the midpoint obviously and the flow field becomes stable relatively when there is very small difference of the exit velocities for opposed jets of $2D \leq L \leq 8D$. At $L < 2D$ or $L > 8D$, the position of stagnation point becomes insensitive to the variety of exit velocity ratio.

Keywords: Opposed jets; Stagnation point offset; CFD; Reynolds stress model; Smoke-wire technique; Hot-wire anemometer

1. Introduction

Due to rapid and high-effective mixing performance, opposed jets have been applied to a number of industrial processes including polymer processing [1,2], drying solid particles [3], absorption [4,5], extraction [6], and rapid chemical reactor [7–9], etc. Early comprehensive reviews on various applications and study advances of opposed jets were presented by Tamir and Kitton [10,11]. However, compared to the numerous industrial applications, the fundamental study on the dynamical characteristics of such flow is still very limited.

Stagnation point offset of two opposed jets has been observed by several researchers in their experiments. Kostiuk et al. [12–14] used laser Doppler velocimetry (LDV) to study the non-reacting flow field of two closely spaced opposed jets. They found that very small differences of the exit flux of the two jets caused the stagnation plane to deviate from the midpoint between the nozzles by up to $0.15D$ at nozzle separation of $2D$. Korusoy and Whitelaw [15] also observed the movement and instability of the stagnation plane at separation above $1.0D$, so that their subsequent investigations were limited to separations between 0.2 and $1.0D$. Lindstedt et al. [16] studied the velocity and strain rate of two opposed isothermal flows experimentally by particle imaging velocimetry (PIV) and numerically by Reynolds stress model. They as well as found that the flows were slightly asymmetric, which became increasingly asymmetrical with reduction in separation. Though stagnation point offset of opposed jets has been observed by several researchers, the fundamental study on the factors affecting it is still very rare.

Kind and Suthanthiran [17] carried out an experimental study on the interaction between two opposed plane turbulent wall jets at $L = 240D$ and found that the position of the interaction depends on the ratio of the momentum fluxes of two wall jets.

Ogawa et al. [18,19] experimentally studied turbulent opposed jets by hot-wire anemometer at two separations of $L = 4.3D$ and $8.57D$. Different to above study, they considered that the impact position was very unstable and not fixed solely by momentum fluxes. Hydrodynamic instabilities and oscillation behaviors of opposed jets have also been observed in the experiments of Rolon et al. [20] and Denshchikov et al. [21,22]. In order to successfully exploit opposed jets for practical applications, it is important to identify the critical parameter values corresponding to transitions from steady state to unstable state.

Due to instabilities and difficulties in alignment and balancing the exit velocities of opposed jets, more researchers performed numerical simulations to investigate the flow characteristics of

* Corresponding author. Tel.: +86 21 64251418.
E-mail address: liweif@ecust.edu.cn (W. Li).

1385-8947/$ – see front matter © 2007 Elsevier B.V. All rights reserved.
doi:10.1016/j.cej.2007.05.039

Nomenclature

a	exit velocity ratio
D	nozzle diameter (m)
L	nozzle separation (m)
Re	jet Reynolds number
u, u_0, u_1, u_2	axial velocity (m s^{-1})
Δx	stagnation point offset (m)
x, y	axial, radial coordinate (m)

Greek letters

μ	dynamic viscosity of air (kg m^{-1} s^{-1})
ρ	air density (kg m^{-3})

unequal opposed jets. Hosseinalipour et al. [23,24] performed numerical simulations of the flow, mixing and thermal characteristics of two steady two-dimensional laminar confined opposed jets for cases when the two jets are equal and unequal. In their work, effects of geometric, hydrodynamic and thermal parameters on the flow and heat transfer characteristics of such system were examined. Johnson [25,26] studied flow characteristic of laminar impingement jets in a confined cylindrical chamber using steady and unsteady three-dimensional numerical simulations. In their work, unequal flow cases in opposed jets indicated an asymmetric flow field and the impingement point was very close to the low flow rate nozzle. Besbes et al. [27] studied two turbulent opposed plane jets having different temperature numerically and found that the stagnation point moves toward the heated jet. Wang et al. [28] examined the mixing effect of unequal laminar confined opposed jets having different inlet momenta numerically. They found these unequal opposed jets caused better mixing effects. Devahastin and Mujumdarb [29] performed a numerical study of flow and mixing characteristics of laminar confined impinging streams. They found that both the inlet jet Reynolds number and the geometry of the system have strong effects on mixing in impinging streams. Up to now, there is very few numerical simulation on the stagnation point offset of turbulent unequal opposed jets in the literature.

Previous studies on stagnation point offset of opposed jets are either of laminar or at one or two specified nozzle separations, and there are some discrepancies of the results of different studies. Moreover, most previous studies on stagnation point offset of opposed jets are mainly focused on the effect of exit velocity ratio, however stagnation point offset at different nozzle separations have never been well studied. In practical applications of opposed jets, there are various nozzle separations: e.g., closely spaced opposed jets ($L<2D$) were commonly used to study the extinction or the kinetic models of the premixed turbulent flames [12–15]; opposed jets of $L=4.76D$ were used in the confined impinging-jets reactors (CIJR) to obtain high mixing efficiency [7–9]; the reaction injection molding (RIM) of opposed jets of $L=6.69D$ was used in the production of plastic components [1,2]; in the application of opposed jets in coal combustion or gasification in large-scale industrial reactor, large nozzle separation ($L>12D$) were commonly used to avoid the ablation of the high temperature flame to the reactor wall [11]. So, we performed experimental study by smoke-wire technique and hot-wire anemometer (HWA) measurements together with numerical simulation to study two axisymmetric and unconfined turbulent opposed jets with equal or unequal exit velocities at $1D \le L \le 20D$. Our objective is to present a comprehensive and fundamental study of the flow characteristics and regularities of stagnation point offset of turbulent opposed jets.

The remainder of this paper is organized as follows: the experiment setup and numerical simulation method are introduced in the following two sections. Results and discussions are presented in Section 4. The paper ends with conclusion in Section 5.

2. Experimental study

2.1. Schematic map of experimental program

The schematic drawing of the stagnation point offset of opposed jets is shown in Fig. 1. Turbulent flow field is obtained by two axisymmetric opposed nozzles with the same geometric configurations as plotted in Fig. 2. The two opposed nozzles are installed in a three-dimensional frame of axes. The diameter D of the nozzle used in the experiment is 30 mm. The exit air velocity ratio α of the two opposed jets is defined as

$$a = \frac{u_2}{u_1} \tag{1}$$

where u_1 and u_2 are the bulk velocities at the exits of nozzles I and II, respectively. In the experiment, the stronger jet is always ejected from nozzle I, so impact point is always close to the exit of nozzle II. Moreover, the exit air velocity of nozzle I is fixed and the exit air velocity of nozzle II is variable. So the exit velocity ratio of the two opposed jets is always less than or equal

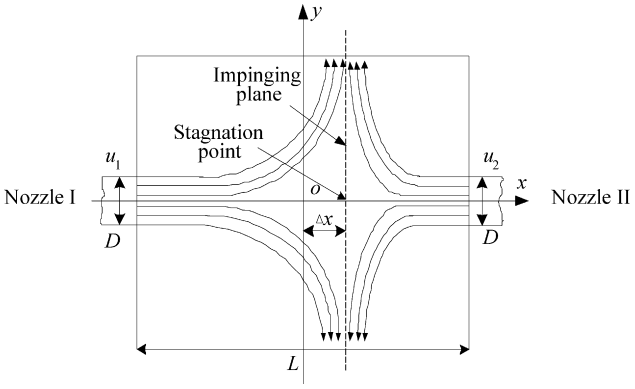

Fig. 1. Schematic map of stagnation point offset of opposed jets.

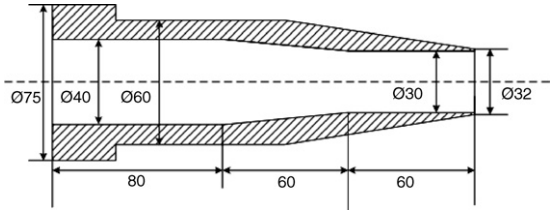

Fig. 2. Cross-section of the nozzle with all dimensions in millimeters.

to 1 in present paper. The distance from the stagnation point to the origin point of the coordinate system is defined as stagnation point offset and denoted by Δx, as marked in Fig. 1.

Quantitative and qualitative experimental studies of the flow field of the opposed jets were carried out with HWA measurements and smoke-wire flow visualization. The jet Reynolds number at the nozzle exit is defined as

$$Re_j = Du_j\rho/\mu \quad (2)$$

where u_j is the bulk velocity of the jet at the nozzle exit; ρ and μ are the density and dynamic viscosity of air under normal conditions. Re_1 and Re_2 are used to describe the jet Reynolds number of the opposed jets ejected from nozzles I and II, respectively.

2.2. Hot-wire anemometer measurement

Mean and rms (root mean square) velocities of the flow field of the opposed jets were measured with a DANTEC hot-wire anemometry system. The probe used was a single wire and sampling frequency was set at 20 kHz and sampling duration was 5 s. The impingement stagnation point was identified by the hot-wire probe even though it could not provide precise measurements of mean and rms velocities in the vicinity of the stagnation plane [30]. This is caused by the inability of the single-sensor probe to distinguish between positive and negative flow fluctuations in the impingement region where mean velocities are low and fluctuation velocities are high. So the measured average velocities are somewhat high and rms velocities are low in the narrow region around the impact point. Our method using the hot-wire probe to determine the position of stagnation point is different to that of Ogawa et al. [18,19]. In their experiment, hot-wire probe was placed 2 cm from the jet center and the position corresponding to the maximum output of the anemometer was considered to be the impact point as probe moved parallel to the axis. In current work, probe was placed along the axis of the opposed jest and the position of minimum mean velocity was defined as the location of the stagnation point. In the measurements, the nozzle separation L is in the region of 30–600 mm and the corresponding normalized nozzle separations L/D range from 1 to 20. The detailed measurement cases are listed in Table 1.

2.3. Smoke-wire technique

The instantaneous flow patterns of equal and unequal opposed jets were visualized by smoke-wire technique. A 0.1 mm diameter stainless steel wire was located across the nozzle exit. The wire was coated by paraffin oil and connected as a resistor to an electric circuit. Then the oil was heated to form smoke by the sudden current when the circuit was on. The flow patterns were photographed intermittently by a Sony DSC-S75 digital camera. The exposure time was set at 0.001 s and more than 30 photos were taken for each case. Smoke-wire technique is limited to relative low exit air velocity and small nozzle separations, otherwise the concentration of smoke is low and the quality of the photo is low. So exit air velocity is in the region of 1.65–2.36 m/s and nozzle separations are from 1D to 8D in present flow visualization. The experimental cases of flow visualization are listed in Table 2.

Table 1
Measurement cases

L (mm)	30, 60, 120, 180, 240, 360, 480, 600
L/D	1, 2, 4, 6, 8, 12, 16, 20
u_1 (m/s)	11.8
a	1, 0.97, 0.9, 0.8, 0.7
Re_1	23,460
Re_2	16,422 ~ 23,460

Table 2
Cases of flow visualization

L (mm)	30, 60, 120, 180, 240
L/D	1, 2, 4, 6, 8
u_1 (m/s)	2.36
a	1, 0.97, 0.9, 0.8, 0.7
Re_1	4692
Re_2	3284 ~ 4692

3. Numerical simulation

The simulations were carried out using a microcomputer (INTEL 2.6 G, 512 MB) with available commercial software (Fluent 6.1). In opposed jets, production of turbulence is attributed to normal strain instead of shear stress with strong effects of streamline curvature and anisotropic. So, some strategies on selecting turbulence model, configuring boundary conditions and testing mesh are necessary.

3.1. Turbulence model

Due to difficulties of experiments, numerical simulations have become an increasingly important approach to study opposed jets with the rapid development of CFD. The generally chosen turbulence models are various versions of two-equation model and RSM. Turbulence and its effects on opposed jets are anisotropic. Instead of using eddy viscosity model for the Reynolds stress, the RSM solves a set of transport equations for the Reynolds stress. It abandons Boussinesq approximations and is able to deal with anisotropy. So, RSM is more preferable to simulate such flow than two-equation models. Champion and Libby [31], Korusoy and Whitelaw [32], Besbes et al. [27], Lindstedt et al. [16] and Chou et al. [33] all confirmed that RSM model predicted better results than various versions of k–ε models in their simulations. So, we selected RSM to simulate the opposed jets in the paper.

3.2. Boundary conditions

The coordinate system, computation domain and boundary conditions are plotted in Fig. 3. The flow field of opposed jets was solved as a two-dimensional axisymmetric flow using the finite volume method. To eliminate the effects of the exit boundary conditions on the flow, the L_{out} and H_{out} of the simulation domain were expanded to $4D + L$ and $11.5D$, respectively. So the distance from pressure outlet boundary to the symmetry axis

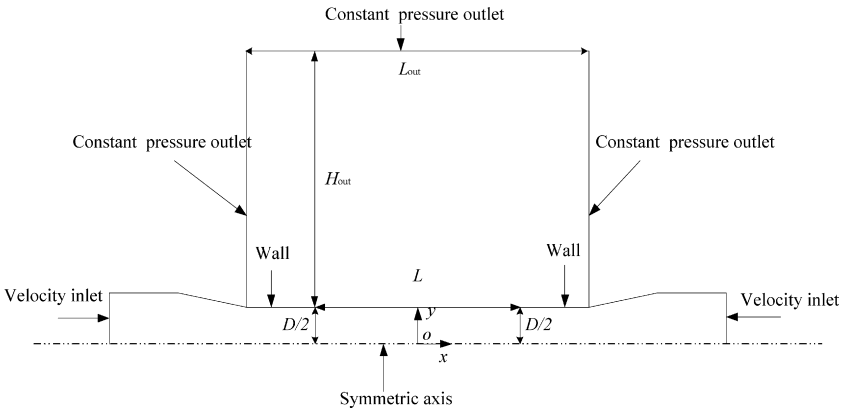

Fig. 3. Solution domain and boundary conditions.

was 12D. Our previous test simulations have proven that the conditions $L_{out} = 4D + L$ and $H_{out} = 11.5D$ are sufficient for all the cases from $L/D = 1$ to 20. Since the inlet of the nozzle was connected to a fully developed turbulent pipe flow, inlet velocity profile distribution was set to follow the seventh power law. And the measured axial velocity profile at the nozzle exit has proved that this inlet configuration was reasonable (see Fig. 12). The inlet values of turbulence intensity and were set to 12% according to the past measurements. Outlet boundary applied constant pressure outlet equal to standard atmosphere pressure (101,325 Pa), so gauge pressure was set to 0.

3.3. Grid tests

According to the chosen turbulent model and boundary conditions, $L = 4D$ was chosen to carry out grid tests at $u_1 = 11.8$ and $a = 0.97$. Four uniform grids: 60×90, 80×120, 120×180 and 240×360 (in the domain $8D \times 12D$) were tested. The dimension of a cell of the finest grid was 1 mm. At the same time, one distributed grid (12,980 nodes) in which smaller grid cells were used in the region of high velocity gradient was also tested to compare with the uniform grids. Test results showed that

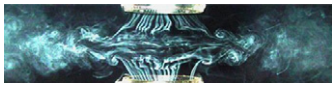

Fig. 4. Photographs of opposed jets at $L = 1D$.

all the five grid did not produce any noticeable change in the axial velocity distribution; and the two coarse uniform grids showed unsatisfactory axial velocity profiles at the nozzle exit and rms velocity at the stagnation plane compared to the two finest uniform grids; and the distributed grid produced profiles and distributions of all calculated quantities that agreed with the two finest uniform meshes and convergence was achieved in one fifth of the time. The distributed grid may be considered as fine enough to provide acceptable, grid independent solutions, so that the distributed grid was used throughout the rest of the calculations in this paper.

The governing equations were discretized using a second order upwind interpolation scheme and the discretized equations were solved using the SIMPLEC algorithm. The solution was considered to be converged when the sum of the normalized residuals for continuity and momentum equations were on the order of 10^{-5}. The test case took about 30 min.

Fig. 5. Photographs of opposed jets at $L = 2D$.

Fig. 6. Photographs of opposed jets at $L = 4D$.

Fig. 7. Photographs of opposed jets at $L = 6D$.

Fig. 8. Photographs of opposed jets at $L = 8D$.

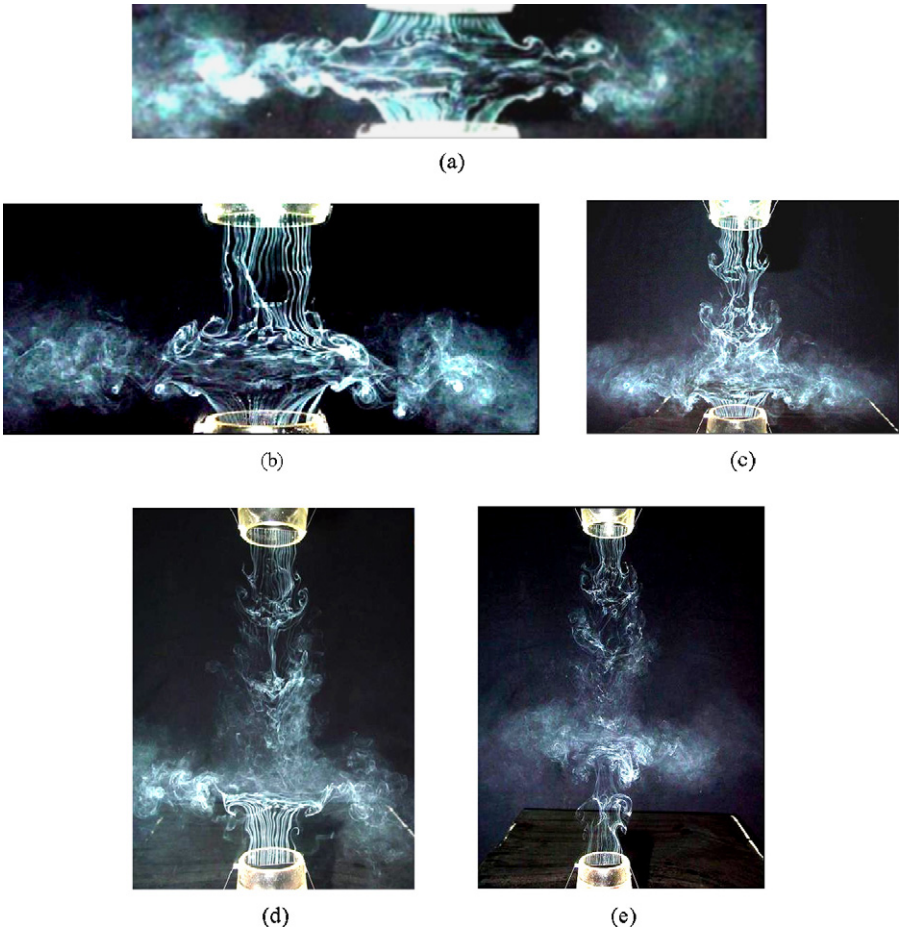

Fig. 9. Photographs of opposed jets with various nozzle separations at $a = 0.97$. (a) $L = 1D$, (b) $L = 2D$, (c) $L = 4D$, (d) $L = 6D$ and (e) $L = 8D$.

4. Results and discussions

4.1. Visualization by smoke-wire technique

In the visualization, u_1 is fixed at 2.36 m/s and exit velocity ratios are 1, 0.97, 0.9, 0.8 and 0.7, respectively. Flow visualization was firstly performed at $u_1 = u_2 = 2.36$ m/s and the normalized nozzle separations of $L/D = 1$, 2, 4, 6 and 8. The selected typical photographs for these cases are given in Figs. 4–8.

At $L/D = 1$, 6 and 8, typical photos show that the impingement planes basically stay at the midpoint of the two nozzles, as shown in Figs. 4, 7 and 8, which indicates that at these nozzle separations, the positions of the stagnation points are stable comparatively.

For separation of $L/D = 2$ and 4, however, the obtained photographs show different patterns as shown in Figs. 5 and 6. We observe that impingement plane stays either at the position near to the top nozzle or at the position near to the bottom nozzle and sometimes the impingement plane shifts rapidly in the region between the two positions. It is very difficult to get impingement stagnation point to stay at the midpoint between the two nozzles, as reported by Kostiuk et al. [12]. The visualization photos indicate that the two positions are stable relatively but the region between them is unstable. The impingement plane shifts rapidly from one stable state to another stable state within the region between the two stable points corresponding to the stable states. So, though we caught the photos as shown in Figs. 5b and 6b, the flow patterns are unstable. It is seen from Figs. 5 and 6 that the locations corresponding to the stable states are at $x = -0.4D$ and $0.4D$ and the unstable region is from $-0.4D$ to $0.4D$ at $L = 2D$ and for $L = 4D$, the region is from $-1.3D$ to $1.3D$. This instability regime is similar to the observation of Rolon et al. [20] but is different to the Denshchikov et al. [21,22]. In the experiment of Rolon et al. [20], they found there were two symmetric stable positions at $x = -0.06D$ and $0.06D$ of the opposed air jets at $L = 1.14D$. However, the length of unstable region in their experiment is much smaller than ours at $L = 2D$ and $4D$. In the experiment of Denshchikov et al. [21,22], they observed oscillatory behavior of two opposed plane water jets under certain conditions. The oscillatory in their experiment was a deflecting jet oscillatory and the two opposed jets were deflected in the opposite direction from each other and switched directions periodically. The difference of the two instability regimes is due to the different geometric configurations of planar and axisymmetric opposed jets. Our experiments can explain the finding of Ogawa et al. [19] that double impact positions sometimes existed. Actually, the double impact positions are the two stable positions of impingement plane on the axis.

The visualization photos of the opposed jets at $a = 0.97$ are shown in Fig. 9a–e. For $a = 0.97$ and $L = 1D$, the impingement plane is still located at the center, which indicates that the position of the stagnation point is insensitive to the small difference of exit velocities of the two nozzles. But at $a = 0.97$ and nozzle separation of $L/D = 2$, 4, 6 and 8, only 3% difference in exit velocities causes stagnation point to deviate from the midpoint between the two nozzles up to $0.4D$, $1.3D$, $2.1D$ and $1.5D$, respectively, as shown in Fig. 9b–e. This implies that the position of the stagnation point is far more sensitive to the exit velocity difference compared to the case of $L/D = 1$. On the other hand, it is also can be seen from these figures that when the impact point deviates from the midpoint, their positions become stable relatively. Just as shown in Fig. 9b–c, for only 3% difference in exit velocities, the flow field becomes stable obviously and the oscillation of the impingement planes is absent.

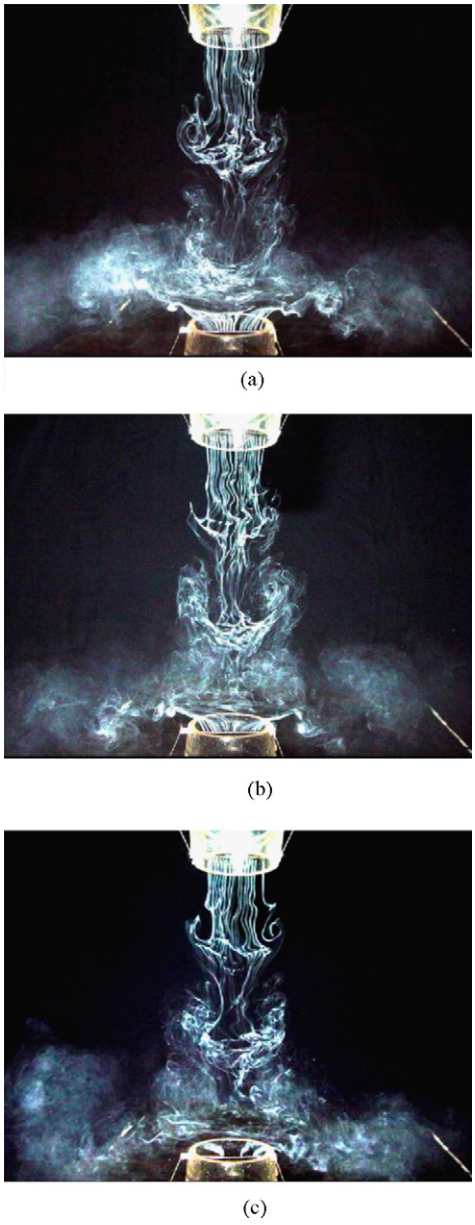

Fig. 10. Photographs of opposed jets with various exit velocity ratio at $L = 4D$. (a) $a = 0.9$, (b) $a = 0.8$ and (c) $a = 0.7$.

Due to the limited pages, the visualization photos of opposed jets with smaller exit velocity ratios are shown in Fig. 10 only for nozzle separation of $L = 4D$. As shown in Fig. 10a–c, with the decrease of exit velocity ratio, the impingement stagnation point moves slowly toward the nozzle having low exit velocity. At small exit velocity ratio, the position of the stagnation point becomes insensitive to the exit velocity ratio, which also

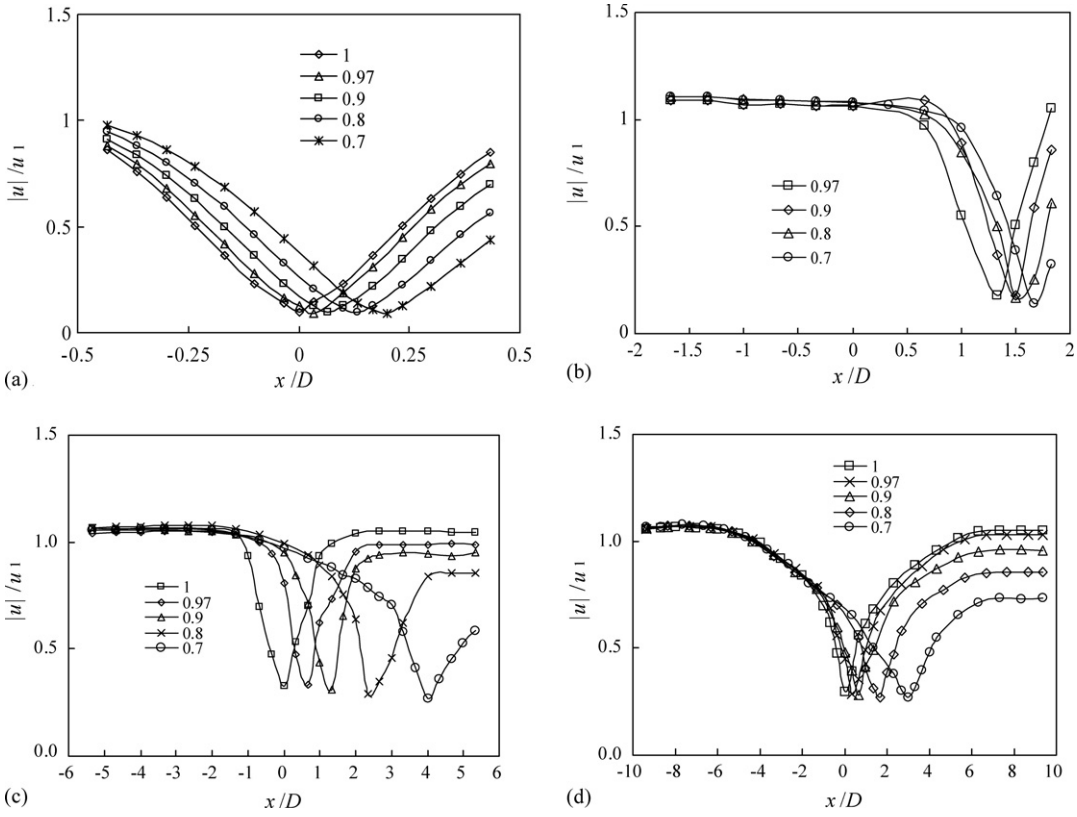

Fig. 11. Distribution of normalized mean axial velocity magnitudes on the axis. (a) $L = 1D$, (b) $L = 4D$, (c) $L = 12D$ and (d) $L = 20D$.

indicates that when impact plane deviates from center, the flow becomes stable relatively. We can also see from Fig. 10 that with the decrease of exit velocity ratio, the impingement plane becomes curving toward the weak jet.

4.2. Results of experimental measurements with HWA

The measured axial velocity distributions of the opposed jets at $L/D = 1$, 4, 12 and 20 are shown in Fig. 11a–d. Though the probe could not identify precisely the position of the stagnation point for few cases, the results is satisfactory generally considering the instability of the opposed jets and the technique used to identify the position of the stagnation point. It must be point out that when the inlet velocities of opposed jets are equal, the impingement plane is unstable and HWA is very difficult to use to measure axial velocities. When the exit velocities of opposed jets are unequal, the flow field becomes stable relatively, so HWA can be used to measure the offset of the stagnation point at $L/D = 4$.

4.3. Results of numerical simulations

The measured and calculated normalized axial mean and rms velocity profiles at 1 mm of the nozzle exit of the single jet at $u_0 = 11.8$ m/s are presented in Fig. 12. It is seen that the nozzles in this experiment have top-hat exit velocity profiles and mean velocity profiles are flat for more than 80% of the nozzle diameter D and the thickness of the boundary layer is about $0.1D$. The normalized rms velocities are constant at about 5% apart from the region within $0.1D$ of the nozzle wall. It is can be seen that the measured and calculated values are in good agreement, which proves that the boundary setting of the numerical model is reasonable.

Fig. 13a–d shows the axial velocities on the axis at $L/D = 4$ and $a = 0.97$, 0.9, 0.8 and 0.7, respectively. The predicted values and the experimental data coincide satisfactorily, though the measured mean velocities in the region adjacent to the stagnation point are somewhat larger than prediction for the reason discussed in Section 2.2.

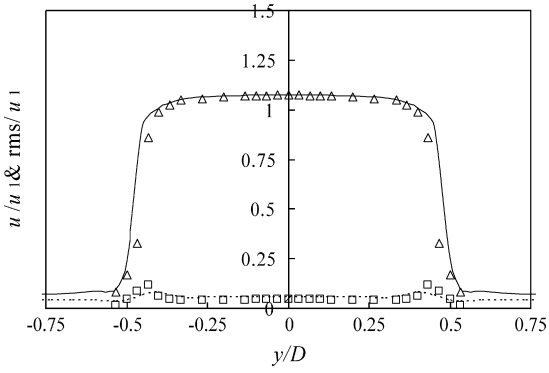

Fig. 12. Distributions of normalized mean and rms axial velocities at nozzle exit of single free jet. Solid line: calculated mean velocity; dashed line: calculated rms velocity. △, measured mean velocity and □, measured rms velocity.

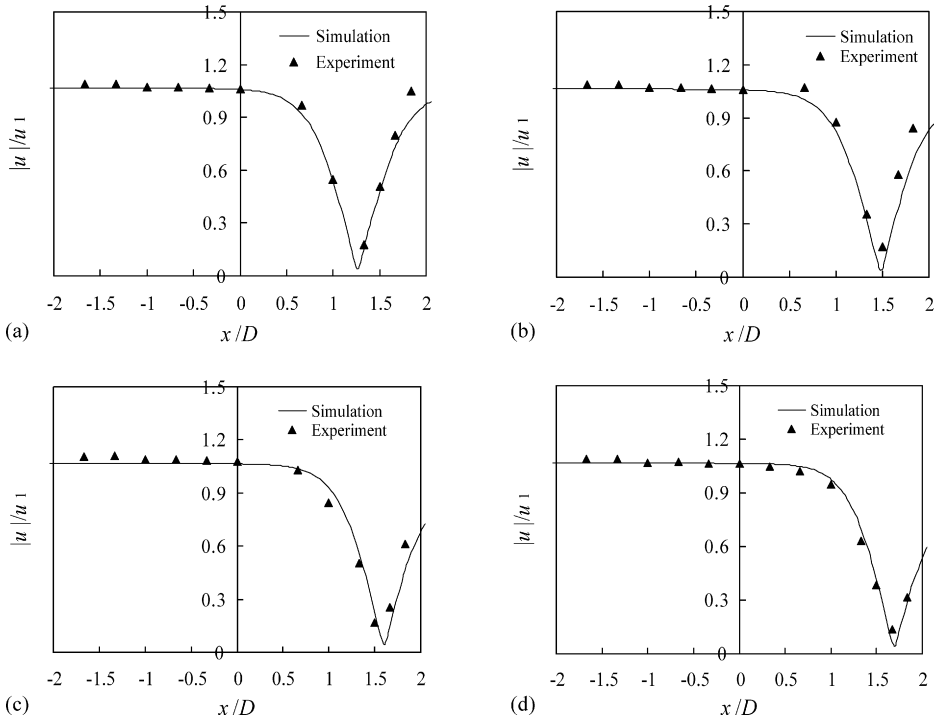

Fig. 13. Measured and simulated axial velocity magnitudes at $L=4D$. (a) $a=0.97$, (b) $a=0.9$, (c) $a=0.8$ and (d) $a=0.7$.

Fig. 14a–e shows the velocity contour maps at $L/D=4$ and $a=1$, 0.97, 0.9, 0.8 and 0.7, respectively. It can be seen from the figures that with the decrease of exit velocity ratio, the impingement plane becomes curving toward the weak jet. It must be point out that because the simulation in this paper is steady, the flow pattern in Fig. 14a is time-averaged and is unstable actually.

At $L/D=1$, 2, 4, 6, 8, 12, 16 and 20, the simulated axial velocity distributions on the axis of various exit velocity ratios are shown in Fig. 15a–h. The axial velocity gradient is found to be approximately homogeneous in the vicinity of the stagnation plane. For the axial velocity distributions with various exit velocity ratios at a certain nozzle separation, the velocity gradient is nearly uniform and the curves parallel in the vicinity of the stagnation plane.

In order to investigate the velocity gradient around the stagnation point of opposed jets at various nozzle separations, we pick out the curves corresponding to $a=1$ in Fig. 15a–h and put them together according to the regions of $L/D<2$, $2\leq L/D\leq 8$ and $L/D>8$, which are shown in Fig. 16a–c. At $L/D>8$ or $L/D<2$, the velocity gradient at the stagnation plane decreases with the increase of nozzle separations, as shown in Fig. 16a and c.

It is interesting to see in Fig. 16b that in the regions of $2\leq L/D\leq 8$, their axial velocity curves overlap each other although they extend within different length of regions on the axis, which means that the velocity gradients are the same. Moreover, if we define the length of the impingement zone is the region in which the axial velocity on the axis is not equal to exit velocity, it can be seen that the lengths of the impingement zones on the axis of opposed jets in the regions of $2\leq L/D\leq 8$ are all equal to $2D$. In the study of Kostiuk et al. [12], they defined the axial bulk strain at the stagnation plane as

$$S_{\mathrm{ax}}=\frac{\partial u}{\partial x} \tag{3}$$

and concluded that the bulk strain rate was increased by a reduction of nozzle separation or an increase in the bulk velocity at $L/D\leq 2$. In our study, axial bulk strain at the stagnation plane decreases with the increase of the nozzle separation at $L/D>8$ or $L/D<2$, which is in agreement with the result of Kostiuk et al. [12]; but in the region of $2\leq L/D\leq 8$, the axial bulk strains near the stagnation plane are nearly constant and about equal to $820\,\mathrm{s}^{-1}$.

It can be seen from Figs. 15 and 16 that in the region of $2\leq L/D\leq 8$, the axial bulk strains near the stagnation plane of all studied a-values are nearly the same.

Stagnation point offsets normalized by D and L at various exit velocity ratios and nozzle separations are shown in Fig. 17a–b. Though there are some discrepancies, numerical simulations are in satisfactory agreement with the experimental measurements. The discrepancies mainly appear at $a=0.97$ when L/D is less than 8, which are caused by the high sensitivity of position of stagnation point to the exit velocity ratio and the error of flux adjusting. Discrepancies also occur at $L/D>12$, especially at $a=0.7$, which may be due to the misalignment of the axes of the two nozzles or the incompetence of the HWA to these more strongly curved flow cases. The maximum discrepancy at $L/D>12$ is $0.667D$ (2 cm), approximately occupying 4.2% of its nozzle separation. It is also should be point out that though flow visualization have described the similar trend of stagnation point offset compared to the measured results, there are still some small disaccords between them. It may results from the

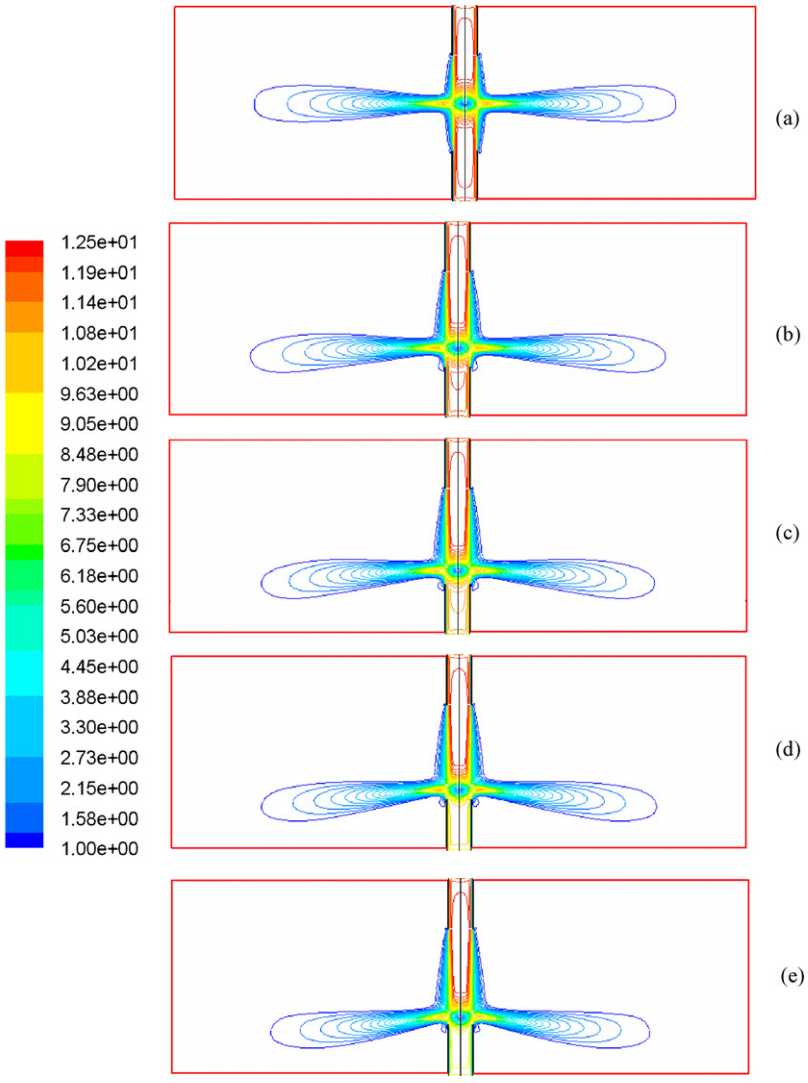

Fig. 14. Velocity contour maps at $L = 4D$. (a) $a = 1$, (b) $a = 0.97$, (c) $a = 0.9$, (d) $a = 0.8$ and (e) $a = 0.7$.

difference of the exit Reynolds number and the influence of exit Reynolds number on the stagnation point offset will be studied in a further work.

It is shown from Fig. 17a that at $L/D = 1$, 12, 16 and 20, the stagnation point offset nearly linearly increases with the decrease of the exit velocity ratio. However, for separations in the region of $2 \leq L/D \leq 8$, stagnation point offset sharply increases at first at $a > 0.9$, and then nearly linearly at $a < 0.9$ with the decrease of the exit velocity ratio, which denotes that at $a > 0.9$, the location of the stagnation point is very sensitive to the small change of the exit velocity ratio.

The stagnation point offset normalized by the nozzle separation versus exit velocity ratio, i.e. $\Delta x/L$ versus a, is shown in Fig. 17b. It is shown from the figure that small difference of exit velocities can cause stagnation point to deviate from the midpoint obviously at $2D \leq L \leq 8D$; as the nozzle separation decreases from $2D$ or increases from $8D$, the degree of stagnation point offset decreases sharply. It denotes that at $2D \leq L \leq 8D$, the stagnation position is very sensitive to the variety of exit velocity ratio but at $L < 2D$ and $L > 8D$, the position of stagnation position becomes insensitive to the variety of exit velocity ratio.

Comparable data in the literature is scarce though stagnation point offset of unequal opposed jets were studied by Hosseinalipour et al. [23,24] and Johnson [25,26] numerically and Ogawa et al. [18,19] experimentally. However, their studies were specified at one or two nozzle separations and different geometry configurations. Johnson [26] studied the flow characteristics of unequal confined laminar opposed jets at $L/D = 10.75$ numerically and found for the exit velocity ratio of 0.47 the stagnation point offset was $4.52D$. The study similar to present work is the experimental research of Ogawa et al. [19]. They found for a exit velocity ratio of 0.94 the stagnation point offset was $1.61D$ (37.44% of the nozzle separation) and for a exit velocity ratio of 0.96 the stagnation point offset was $1.32D$ (30.7% of the nozzle separation) at $L/D = 4.3$. Their results also reveal the nonlinear relation between exit velocity ratio and the stagnation point offset as discussed in the present work. Their values is consistent to the values at $L/D = 4$ in the present work.

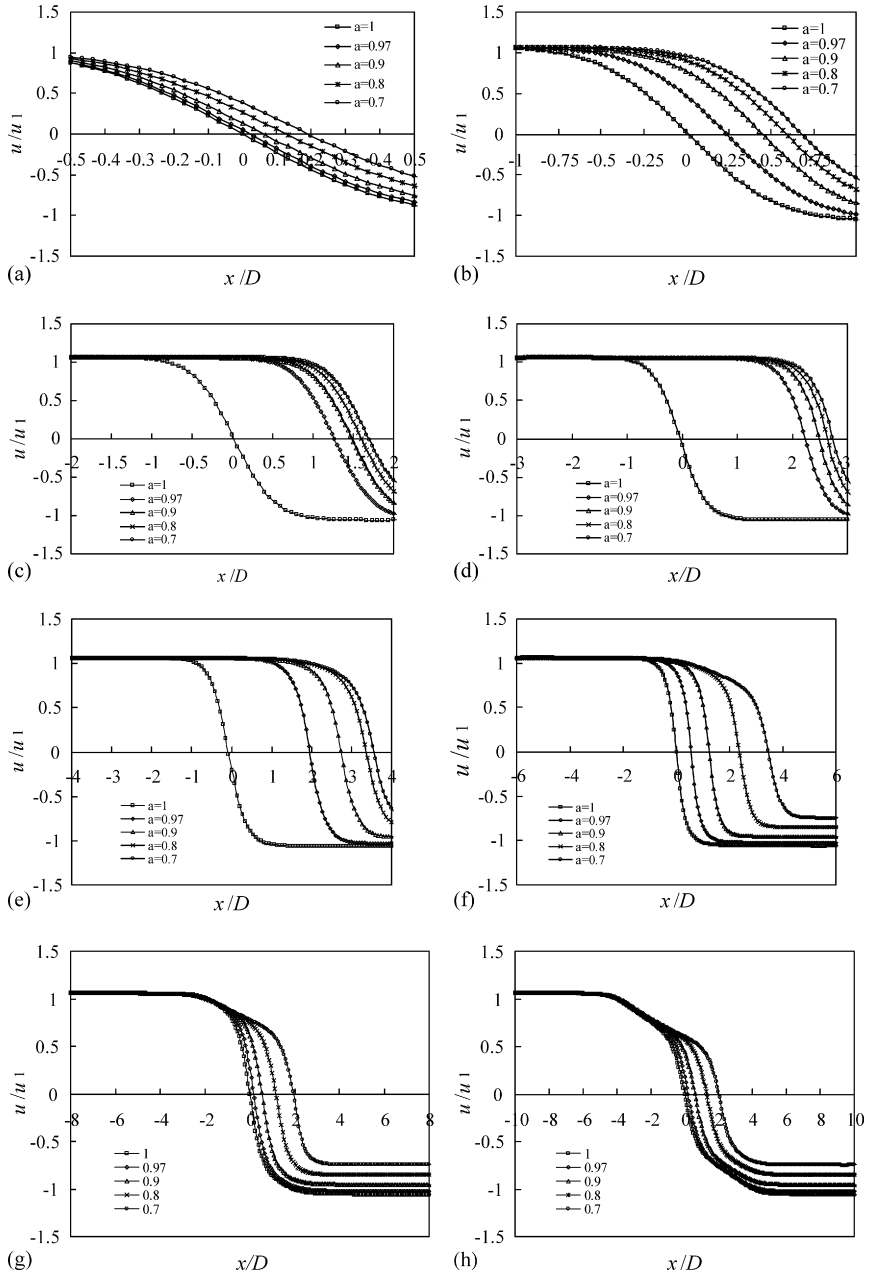

Fig. 15. Axial velocity distributions at various exit velocity ratios and nozzle separations. (a) $L = 1D$ (b) $L = 2D$, (c) $L = 4D$ (d) $L = 6D$, (e) $L = 8D$ (f) $L = 12D$, (g) $L = 16D$ and (h) $L = 20D$.

In the study of Kind and Suthanthiran [17], they found that the stagnation position depends on the ratio of the momentum fluxes of two wall jets at large nozzle separation. In their study, the stagnation point position moved uniformly to the weaker jet with the decrease of the ratio of the momentum fluxes of two wall jets. Though the nozzle and nozzle separation of their study are different to us, their conclusion is similar to the results of opposed jets of $L/D < 2$ or $L/D > 8$ in the present work.

Though we have known the different behaviors of stagnation point movement at various nozzle separations and exit velocity ratios, how to explain the difference of stagnation point offset at various nozzle separations is still very difficult. By carefully investigating the photos of flow visualization, we think the difference may be due to the large-scale vortexes in the boundary layers of the jets caused by the Kelvin–Helmholtz shear instability. These large-scale vortexes are instable [34]. As shown in the visualization photos, after an "undisturbed length", there are axisymmetric vortex rings appearing in the boundary layers of the jets, which grow in size downstream, rotate towards and away from the axis. For opposed jets of $L < 2D$, before impingement the large-scale vortices do not form in the axial shear layers of the two opposed jets and the jets are in the "undisturbed zone" [35]. For opposed jets of $L > 8D$ or more, these axial large-scale vortices in the boundary layers will be broken into small vortices and jets enter the fully developed

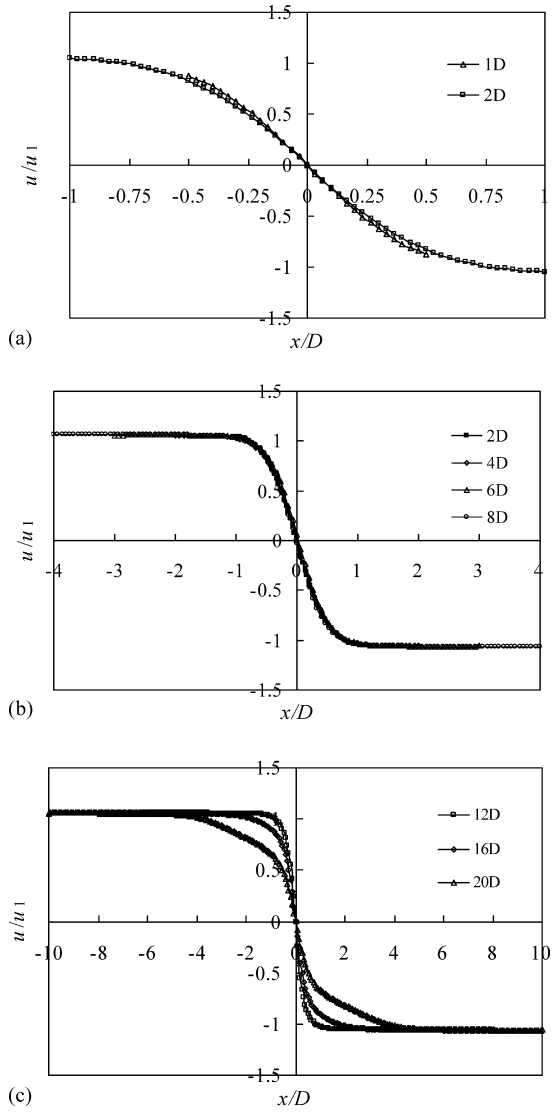

Fig. 16. Axial velocity distributions of various nozzle separations at $a = 1$. (a) $L \leq 2D$, (b) $2D \leq L \leq 8D$ and (c) $12D \leq L \leq 20D$.

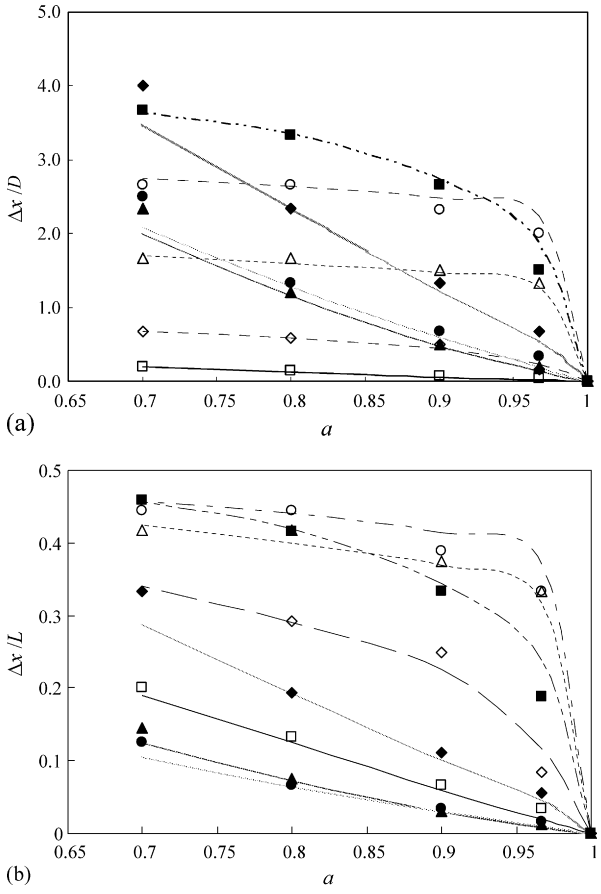

Fig. 17. Normalized stagnation point offset at various exit velocity ratios and nozzle separations. Scatter symbols: measurements—□, 1D; ◊, 2D; △, 4D; ◯, 6D; ■, 8D; ♦, 12D; ▲, 16D; ●, 20D. Line: simulations, —: 1D; – – – –: 2D; · · ·: 4D; – · – · –: 6D; - · - · -: 8D; ▭▭▭: 12D; ▭▭▭▭▭: 16D; ……: 20D. (a) $\Delta x/D$ vs. a, (b) $\Delta x/L$ vs. a.

zone before the two jets impact each other. For these two cases, the large-scale instability has weak influence on the stagnation point offset, so the position of the stagnation point is insensitive to the small difference of the exit velocities. But for opposed jets in the regions of $2 \leq L/D \leq 8$, impingement is in the region of the jets where axial large-scale vortices exist, so the large-scale instability has strong influence on the stagnation point offset.

According to the characteristics of stagnation point offset at the various nozzle separations studied in current paper, we can classify the opposed jets into three kinds: small separation ($L < 2D$), moderate separation ($2 \leq L/D \leq 8$) and large separation ($L > 8D$). For opposed jets of small and large separations, the position of the stagnation point is insensitive to the difference of the nozzle exit velocities, but at the moderate separation, a small difference of the exit velocities causes obvious offset of stagnation point.

5. Conclusion

The stagnation point offset of opposed jets at various exit velocity ratios and nozzle separations were studied experimentally by HWA and smoke-wire technique, and numerically by CFD. The main conclusions can be summarized as follows:

(1) At $2D \leq L \leq 4D$, the stagnation point position of opposed jets with equal exit velocities is instable and oscillates within a region between two relative stable points; it deviates from the midpoint obviously caused by small difference of exit velocities and the flow field becomes stable comparatively.
(2) At $L/D > 8$ or $L/D < 2$, the axial velocity gradient decreases with the increase of nozzle separation, but in the regions of $2 \leq L/D \leq 8$, the velocity gradient and length of the impingement zone on the axis are the same.
(3) For opposed jets at $L/D < 2$ or $L/D > 8$, the stagnation point offset increases nearly linearly with the decrease of the exit velocity ratio, but for opposed jets in the region of $2 \leq L/D \leq 8$, the relationship between the stagnation point offset and the exit velocity ratio is nonlinear. For opposed jets in this region, the stagnation point offset increases

sharply with the decrease of the exit velocity ratio then increases slowly at large exit velocity ratio.

(4) The instability and sensitivity of the stagnation point offset to the small difference of the exit velocities of opposed jets may ascribe to the instability of the large-scale vortices in the boundary layers of opposed jets.

The study of the stagnation point offset of impinging streams is crucial for the effective use of such flow in industrial applications, because imbalance of the exit flux of impinging streams is inevitable practically. The most important find of our study is that there exists a region of $2D \leq L \leq 8D$, in which the stagnation point of opposed jets is very sensitive to the exit velocity ratio, and small difference (3% or less) of exit velocity can cause the stagnation point to deviate obviously. For smaller and larger nozzle separations, the location of stagnation point becomes much more insensitive to the exit velocity ratio.

Acknowledgments

This study was supported by the National Development Programming of Key Fundamental Researches of China (2004CB217703), Program for New Century Excellent Talents in University (NCET-05-0413), and Program for Changjiang Scholars and Innovative Research Team in University.

References

[1] A.M. Teixeira, R.J. Santos, M.R.P. Costa, Hydrodynamics of the mixing head in RIM: LDA flow-field characterization, AIChE J. 51 (2005) 1608–1619.
[2] R.J. Santos, A.M. Teixeira, J.C.B. Lopes, Study of mixing and chemical reaction in RIM, Chem. Eng. Sci. 60 (2005) 2381–2398.
[3] S.M. Hosseinalipour, A.S. Mujumdar, Flow, heat transfer and particle drying characteristics in confined opposing turbulence jets: a numerical study, Dry. Technol. 13 (1995) 753–781.
[4] Y. Berman, A. Tanklevsky, Y. Oren, A. Tamir, Modeling and experimental studies of SO2 absorption in coaxial cylinders with impinging streams. Part I, Chem. Eng. Sci. 55 (2000) 1009–1021.
[5] Y. Berman, A. Tanklevsky, Y. Oren, A. Tamir, Modeling and experimental studies of SO2 absorption in coaxial cylinders with impinging streams. Part II, Chem. Eng. Sci. 55 (2000) 1023–1028.
[6] A.M. Dehkordi, A novel two-impinging-jets reactor for copper extraction and stripping processes, Chem. Eng. J. 87 (2002) 227–238.
[7] B.K. Johnson, R.K. Prud'homme, Chemical processing and micromixing in confined impinging jets, AIChE J. 49 (2003) 2264–2282.
[8] Y. Liu, R.O. Fox, CFD predictions for chemical processing in a confined impinging-jets reactor, AIChE J. 52 (2006) 731–744.
[9] E. Gavi, D.L. Marchisio, A.A. Barresi, CFD modelling and scale-up of confined impinging jet reactors, Chem. Eng. Sci. 62 (2007) 2228–2241.
[10] A. Tamir, A. Kitton, Application of impinging streams in chemical engineering process review, Chem. Commun. 50 (1987) 241–330.
[11] A. Tamir, Impinging-Stream Reactors: Fundamentals and Applications, Elsevier, Amsterdam, 1994.
[12] L.W. Kostiuk, K.N.C. Bray, R.K. Cheng, Experimental study of premixed turbulent combustion in opposed streams. Part I. Nonreacting flow field, Combust. Flame 92 (1993) 377–395.
[13] L.W. Kostiuk, K.N.C. Bray, R.K. Cheng, Experimental study of premixed turbulent combustion in opposed streams. Part II. Reacting flow field and extinction, Combust. Flame 92 (1993) 396–409.
[14] L.W. Kostiuk, I.G. Bray, K.N.C. Bray, Experimental study of premixed turbulent combustion in opposed streams. Part III. Spatial structure of flames, Combust. Flame 118 (1999) 129–139.
[15] E. Korusoy, J.H. Whitelaw, Extinction and relight in opposed flames, Exp. Fluids 33 (2002) 75–89.
[16] R.P. Lindstedt, D.S. Luff, J.H. Whitelaw, Velocity and strain-rate characteristics of opposed isothermal flows, Flow Turbul. Combust. 74 (2005) 169–194.
[17] R. Kind, K. Suthanthiran, The interaction of opposing plane turbulent wall jets, J. Fluid Mech. 58 (1973) 389–402.
[18] N. Ogawa, H. Maki, Studies on opposed turbulent jets (influences of a body on the axis of opposed turbulent jets), Bull. JSME 29 (1986) 2872–2877.
[19] N. Ogawa, H. Maki, K. Hijikata, Studies on opposed turbulent jets (impact position and turbulent component in jet center), Int. J. JSME 35 (1992) 205–217.
[20] J.C. Rolon, D. Veynante, J.P. Martin, Counter jet stagnation flows, Exp. Fluids 11 (1991) 313–324.
[21] V.A. Denshchikov, V.N. Kontratev, A.N. Romashev, Interaction between two opposed jets, Fluid Dynam. 6 (1978) 924–926.
[22] V.A. Denshchikov, V.N. Kontratev, A.N. Romashev, V.M. Chubarov, Auto-oscillations of planar colliding jets, Fluid Dynam. 3 (1983) 460–462.
[23] S.M. Hosseinalipour, A.S. Mujumdar, Flow and thermal characteristics of steady two dimensional confined laminar opposing jets. Part I. Equal jets, Int. Commun. Heat Mass Transfer 24 (1997) 27–38.
[24] S.M. Hosseinalipour, A.S. Mujumdar, Flow and thermal characteristics of steady two dimensional confined laminar opposing jets. Part II. Unequal jets, Int. Commun. Heat Mass Transfer 24 (1997) 39–50.
[25] D.A. Johnson, Experimental and numerical examination of confined laminar opposed jets. Part I. Momentum balancing, Int. Commun. Heat Mass Transfer 27 (2000) 443–454.
[26] D.A. Johnson, Experimental and numerical examination of confined laminar opposed jets. Part II. Momentum imbalance, Int. Commun. Heat Mass Transfer 27 (2000) 455–463.
[27] S. Besbes, H. Mhiri, L.P. Georges, P. Bournot, Numerical and experimental study of two turbulent opposed plane jets, Heat Mass Transfer 39 (2003) 675–686.
[28] S.J. Wang, S. Devahastin, A.S. Mujumdar, A numerical investigation of some approaches to improve mixing in laminar confined impinging streams, Appl. Therm. Eng. 25 (2005) 253–269.
[29] S. Devahastin, A.S. Mujumdarb, A numerical study of flow and mixing characteristics of laminar confined impinging streams, Chem. Eng. J. 85 (2002) 215–223.
[30] E. Korusoy, J.H. Whitelaw, Opposed jets with small separations and their implications for the extinction of opposed flames, Exp. Fluids 31 (2001) 111–117.
[31] M. Champion, P.A. Libby, Reynolds stress description of opposed and impinging turbulent jets. Part I. Closely spaced opposed jets, Phys. Fluids A 5 (1993) 203–216.
[32] E. Korusoy, J.H. Whitelaw, Inviscid, laminar and turbulent opposed jets, Int. J. Numer. Meth. Fluids 46 (2004) 1069–1098.
[33] C.P. Chou, J.Y. Chen, J. Janicka, E. Mastorakos, Modeling of turbulent opposed-jet mixing flows with k–ε model and second-order closure, Int. J. Heat Mass Transfer 47 (2004) 1023–1035.
[34] B. Castaing, P. Huerre, M. Rossi, Hydrodynamics and Nonlinear Instabilities, Cambridge University Press, Cambridge, 1998.
[35] J. Lasheras, E. Hopfinger, Liquid jet instability and atomization in a coaxial gas stream, Annu. Rev. Fluid Mech. 32 (2000) 275–308.